Cellulose (2023) 30:6471–6486
https://doi.org/10.1007/s10570-023-05284-8

ORIGINAL RESEARCH

Air filters fabricated by fibrillated lyocell fibres and polyethylene terephthalate fibres with implantation of cellulose nanofibrils for high-efficiency particulate matter removal

Jiawei Zhang · Xiaojun Wang · Huicheng Huang · Bin Zhang · Hao Zhou · Yujun Xin · Guangting Han · Yuanming Zhang

Received: 24 November 2022 / Accepted: 23 May 2023 / Published online: 5 June 2023

Abstract Air pollution has become a serious threat to human health; hence, it is highly desirable to develop high-efficiency air filters. In this paper, porous cellulose nanofibril (CNF)-implanted air filters with hierarchical structures consisting of LC/PET/CNF composites were prepared using pressurized filtration. The frame of the composite was made of fibrillated lyocell fibres (LC), while polyethylene terephthalate (PET) fibres acted as spacers between the fibrillated LC fibres. CNFs serving as functional fillers were implanted in the LC/PET composite to decrease pressure drop. The results showed that the overall filtration efficiency of the LC/PET composite (50%:50%) with a basis weight of 30 g/m^2 for particulate matter (PM) was only 52.69%, while the pressure drop was 56.50 Pa. However, after implantation of CNFs in the LC/PET composite with a weight concentration of only 0.5 g/m^2, the overall filtration efficiency significantly improved to 98.22% with an acceptable pressure drop of 145.50 Pa ($P_{50}W_{30}t_3N_{0.5}$). The study provides a new way to achieve high-efficiency fabrication of air filters with high performance for PM removal.

Jiawei Zhang and Xiaojun Wang have contributed equally to this work.

Supplementary Information The online version contains supplementary material available at https://doi.org/10.1007/s10570-023-05284-8.

J. Zhang · H. Huang · B. Zhang · H. Zhou · Y. Xin (✉) · G. Han
College of Textiles & Clothing, Qingdao University, Qingdao, Shandong 266071, People's Republic of China
e-mail: xinyujun66@163.com

X. Wang · G. Han · Y. Zhang (✉)
State Key Laboratory of Bio-Fibres and Eco-Textiles, Qingdao University, No. 308 Ningxia Road, Qingdao, Shandong 266071, People's Republic of China
e-mail: zhangyuanming001@163.com

Graphical abstract

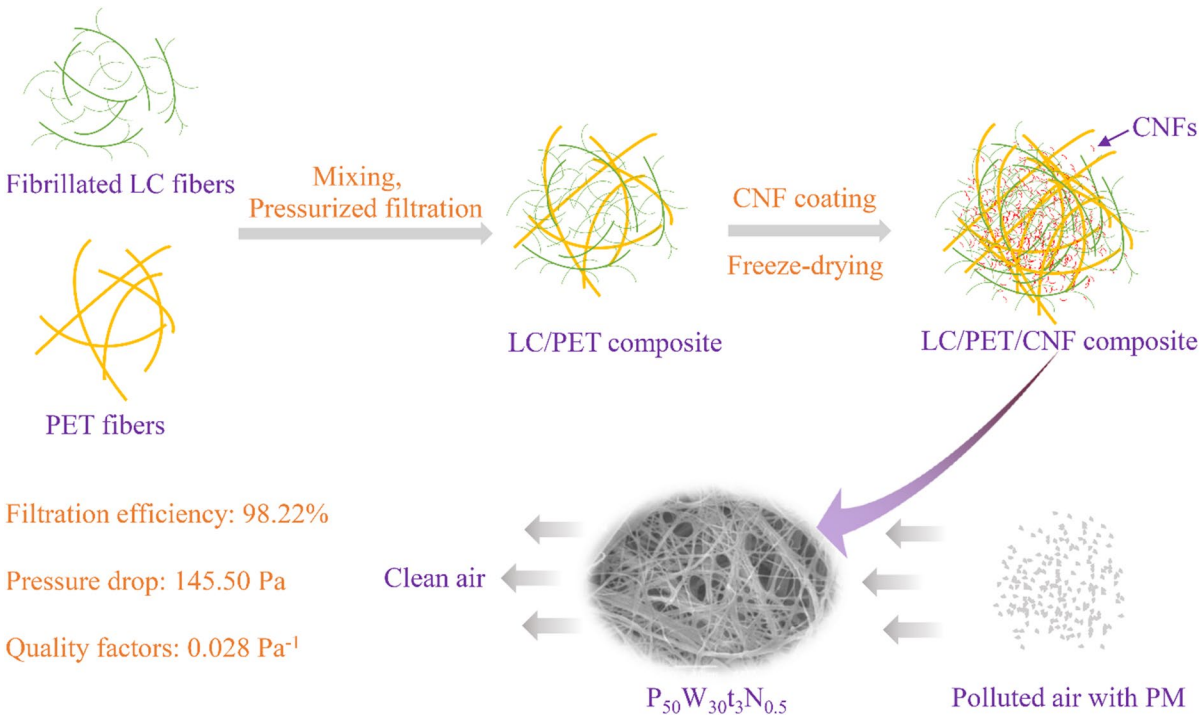

Keywords Fibrillated fibres · Cellulose nanofibrils · Hierarchical structure · Air filtration · Filtration efficiency

Introduction

Air in certain areas is highly polluted by particulate matter (PM), gases (e.g., carbon dioxide, CO_2; carbon monoxide, CO; formaldehyde, HCHO) (White et al. 2019; Wang et al. 2022a), and microbial pollutants, which strongly affect air quality and human health (Ma et al. 2018). Among the various types of air pollutants, PM has been shown to have harmful effects on human health. It is well known that PM is classified into $PM_{2.5}$ (PM with size ≤ 2.5 μm) and PM_{10} (PM with size ≤ 10 μm) based on size (Souzandeh et al. 2017). PM_{10} can enter people's lungs through inhalation because it is small, leading to potential health risks (Ren et al. 2021). $PM_{2.5}$ is one of the most hazardous pollutants because it can permeate bronchi, extrapulmonary organs and possibly the central nervous system through the bloodstream, causing premature death (Zhang et al. 2016). Efficient removal of hazardous materials from the environment has become an important issue from biological and environmental perspectives. Air pollution not only poses risks to public health but also severely limits the sustainable development of societies (Wu et al. 2018). Hence, air pollution remediation has become an important issue.

Air filters show great potential for the remediation of air pollution because they can effectively remove PM. Electrospinning technology for preparing air filters has attracted intensive attention. Polymers such as polyacrylonitrile (PAN) (Wang et al. 2020a, b, c), polyimide (PI) (Gu et al. 2017), poly(vinyl alcohol) (PVA) (Watanabe et al. 2018), polypropylene (PP) (Kiss et al. 2020), polystyrene (PS) (Park et al. 2022), poly(vinyl alcohol) (PVA) (Wang et al. 2021), and cellulose (Han et al. 2008; Balgis et al. 2017; Long et al. 2018) have been used in air filters by electrospinning technology, through which fibrous filters can be developed

with micrometre-sized diameters, high specific surface areas and tuneable porous structures such as spider-like fibrous filters (Pant et al. 2013), lotus-leaf fibrous filters (Shi et al. 2022), tubular fibrous filters (Xu et al. 2021) and tree-like fibrous filters (Maiti et al. 2013). Owing to their special hierarchical structures with submicron and nanosize fibres, filters manufactured by electrospinning usually possess high filtration efficiency and low pressure drops (Avossa et al. 2021; Wang et al. 2022b). Although some advances have been realized in developing high-efficiency electrospun air filters, the electrospinning method has limitations in achieving large-scale production because it requires a high voltage input. Due to their abundant pores and light weight, aerogels fabricated by freeze-drying or supercritical drying have also been considered an efficient way to develop air filters (Nata et al. 2014; Lavoine and Bergström 2017) (Wang et al. 2022b). The hierarchical porous structure of an air filter prepared by freeze-drying can be readily regulated by changing fabrication conditions. Qin et al. reported a dual ice-templating assembly method to govern the assembly of CNFs (Qin et al. 2021). CNFs were first assembled into submicron fibres at − 196 °C, followed by construction of a hierarchical lamellar fibrous structure at − 20 °C. The obtained lamellar fibrous aerogel demonstrated great promise in the air filtration field. However, freeze-drying is a high-energy fabrication method, and thus, the preparation of many aerogels is limited to the laboratory scale. Recently, classical paper-making, vacuum, and pressurized filtration strategies for the fabrication of air filter composites have been widely employed owing to their great potential in commercialization (Wang et al. 2022b). However, the main drawback of this preparation method is poor filter permeability. Substantial efforts need to be made to improve the permeability of air filters while maintaining high filtration efficiency.

CNFs represent a new generation of biopolymers that show favourable biodegradability (Thakur and Thakur 2014) and sustainability (Tu et al. 2021). Currently, CNFs are attractive for many applications, such as filters (Xiong et al. 2022), packaging materials (Wang et al. 2020a, b, c), food stabilizers (Li et al. 2021), oil drilling fluids (Heggset et al. 2017), and coatings and paintings (Hoeng et al. 2016), because of intrinsic properties such as high specific surface area (Wang et al. 2020a, b, c), good mechanical strength (Farooq et al. 2019) and surface modifiability (Navarro et al. 2016, 2020; Beaumont et al. 2018). In this study, a porous air filter based on an LC/PET composite was constructed using a pressurized filtration method, and CNFs were subsequently embedded in the composite to achieve highly efficient PM removal. Lyocell fibres were fibrillated by blending in a blender, and the effect of blending conditions on the morphologies and sizes of the fibrillated fibres was explored. The PET fibres were mixed with a fibrillated LC fibre suspension to construct air filter composites to reduce the pressure drop. The effect of various levels of fibrillated fibres, basis weight of composites and fibrillated LC fibres/PET fibres ratio on filtration efficiency and pressure drop of air filter composites was revealed. In an effort to improve filtration efficiency and reduce pressure drop, CNFs were embedded in the LC/PET composite to construct a hierarchical structure. The objective of this study is to demonstrate a method to build an air filter composite with high PM removal efficiency as well as relatively lower pressure drop. This study may offer an efficient and promising method for the development of air filer composites.

Materials and methods

Materials

Lyocell fibres with a diameter of 14.86 μm and polyester fibres with 0.8% polyoxyethylene (PEO) were provided by Changnuo New Material Technology Co., Ltd. (Shandong, China). The polyester fibres have excellent physical and mechanical properties. They have a chemical formula of $(C_{10}H_8O_4)_n$, and the chemical structure is shown in Fig. S5. Anionic polyacrylamide (APAM, AR) with a molecular weight of 1.2×10^7 Da was purchased from Zhiyuan Chemical Reagent Co., Ltd. (Tianjin, China). Sodium hydroxide (AR) was obtained from Aladdin Co., Ltd. (Shanghai, China). Polypropylene microporous membranes with 0.45 μm pore diameters and 200 mm diameters were provided by Sanqing Filtration Equipment Manufacturing Co., Ltd. (Jiangsu, China). Isopropanol (IPA, AR) was produced by Sinopharm Chemical Reagent Co., Ltd. (Shanghai, China). Samples of CNFs were purchased

from ScienceK Ltd. (Shanghai, China) and were prepared using TEMPO-mediated oxidation. The primary hydroxyls on the surface of cellulose were oxidized to carboxylate groups. Bleached softwood pulp was used without pretreatment as the raw material for CNF production. The diameter of the CNFs ranged from 5 to 20 nm, while their length was between 1 and 3 μm. All chemicals were used as received without further purification.

Fibrillation of lyocell fibres

Sodium hydroxide was employed to swell the lyocell fibres to facilitate its subsequent fibrillation. In detail, 2 wt% sodium hydroxide solution was added to 0.1 wt% lyocell fibres suspended in deionized water. Then, the fibres were placed in a water bath (HH-4, China) at 60 ℃ for 24 h. Next, the fibres and sodium hydroxide solution were separated using a 250 mesh screen. The obtained samples were washed with deionized water repeatedly until they were neutral. The obtained lyocell fibres were labelled S_x, with S representing the sodium hydroxide treatment and x being the sodium hydroxide concentration.

The swollen lyocell fibres were then mechanically treated by a Broken Wall Cooking Machine blender (HX-901, Jincai Electrical Appliance Factory, China) for different amounts of time under various blending rates. APAM (0.2 wt%) was added as a surfactant to improve the dispersion of lyocell fibres in water. The fibre concentration was 0.1 wt% or 0.4 wt%. The obtained fibrillated lyocell fibres were denoted $S_xC_yR_at_b$, with C being the concentration of lyocell fibres in y wt%, R representing the blending rate at a revolutions and t standing for mechanical treatment time over b min. For the revolution term a, the values of 1, 2 and 3 represent 12,000, 24,000 and 36,000 r/min, respectively.

Fabrication of LC/PET composites

PET fibres were suspended in deionized water at a concentration of 0.05 wt% under stirring at 400 r/min for 5 min. Then, they were mixed with fibrillated lyocell fibres under stirring at 400 r/min for 30 min. The well-dispersed mixtures obtained were used to construct LC/PET composites using the pressurized filtration equipment shown in Fig. S1 (SQ-200, Sanqing Filtration Equipment Manufacturing Co., Ltd, China). The composites were filtered through a polypropylene microporous membrane with a pore diameter of 0.45 μm. The composites were labelled $P_cW_dt_e$, with c being the percentage of fibrillated lyocell fibres in the composites, d representing the basic weight of the composites and e representing the blending time. The preparation of fibrillated lyocell fibres and fabrication of composites are schematically shown in Fig. 1.

Spray coating of CNFs on LC/PET composites

The suspension of CNFs at a 0.05 wt% concentration was sprayed on the selected LC/PET composites that served as the substrate using a spray nozzle. The spraying conditions were controlled by controlling the distance between the nozzle and the composite. Then, the acquired samples were immersed in liquid nitrogen for 2 min and subsequently placed in a freeze-dryer (CTFD-10S, China) for 48 h to obtain LC/PET/CNF composites that were denoted as $P_cW_dt_eN_f$, with N representing the addition of CNFs at a dose of f g/m^2.

Characterization of the morphology of fibres and the pore size distribution and density of composites

Optical microscopy (OM, BX51TF, Japan) was employed to characterize the morphology of the lyocell fibres and PET fibres. The diameters of the lyocell and PET fibres were measured based on 3 to 5 optical microscopy images using Nanomeasurer software (Shanghai, China), and each set of approximately 100 measurements was used to count the average diameter. The surface of the composites was observed with scanning electron microscopy (SEM, Zeiss, Germany) at an accelerating voltage of 15 kV. The composite was first cut into 4×4 mm^2 pieces and then attached to the conductive adhesive on a sample platform. The surface of the composites was gold-coated prior to SEM observation. The pore size distribution of the composites was quantitatively determined using a pore size distribution instrument (PSM165 TOPAS, Germany), and three replicates were prepared for each group of tests. IPA was used as a test fluid to determine the pore size distribution. The thickness of the composites (δ) was measured using a thickness tester (CHY-C2A, Labthink, China). Ten points were randomly selected and measured.

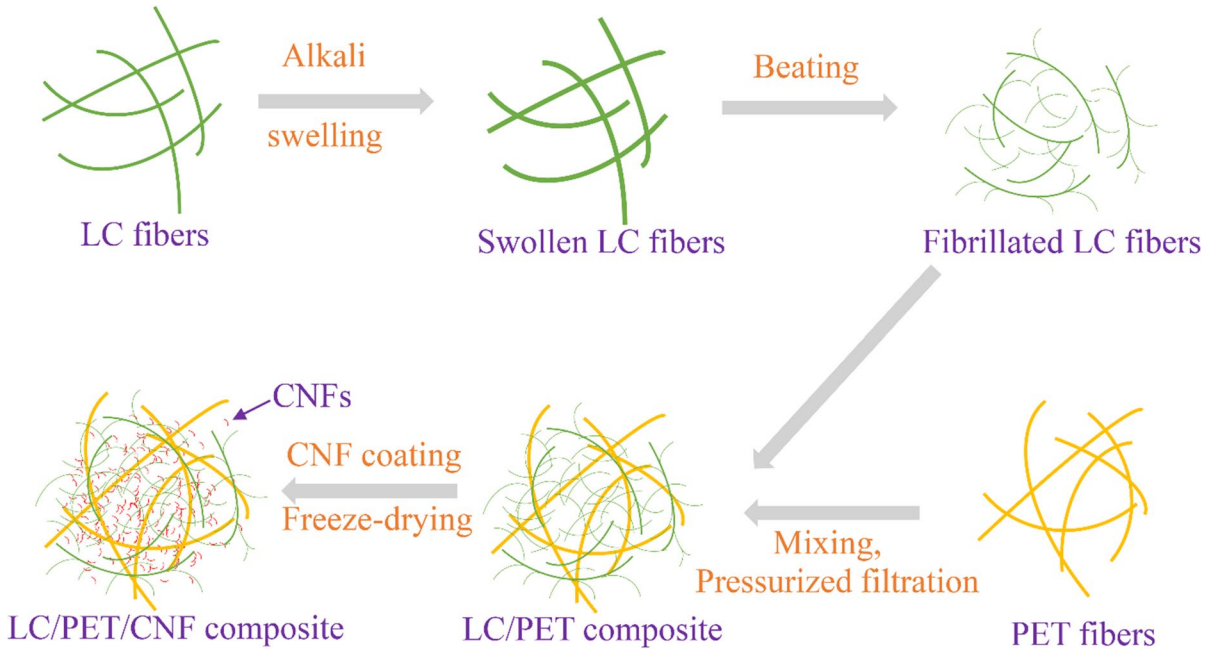

Fig. 1 Schematic illustration of the preparation of fibrillated lyocell fibres and the fabrication of composites

The volume (V) of the composites was determined according to Eq. (1),

$$V = \mathrm{p}R^2\delta \tag{1}$$

where R is the radius of the composite, and R = 90 mm.

The density (ρ) of the composites was calculated according to Eq. (2),

$$\rho = m/v \tag{2}$$

where m is the dry mass of the composite.

BET

The N_2 adsorption–desorption isotherms were determined with an ASAP 2460 automated instrument (Micromeritics, USA). The specific surface area of composites of $P_{50}W_{30}t_3$, $P_{50}W_{30}t_3N_{0.25}$ and $P_{50}W_{30}t_3N_{0.5}$ was obtained based on the BET method, while their pore size distribution and pore volume were calculated according to the BJH method. The composites were degassed at 299 K for 6 h prior to measurements.

Mechanical properties

The mechanical properties of the air filters were tested using a universal testing machine (3382, INSTRON) with a 0.25 kN load cell. Rectangular strips with dimensions of 15 × 40 mm^2 were cut from the composite, and the crosshead speed was 100 mm/min. The reported tensile strength and Young's modulus correspond to the average values of at least 5 measurements.

Filtration performance

Filtration tests were carried out using a filter performance tester (AFC131 TOPAS, Germany) (Fig. S6) at 24 °C and under different relative humidities (RHs) of 20–90%. NaCl and DEHS aerosol particles with diameters of 0.2–0.35 μm, 0.35–0.6 μm,

0.6–1 μm, 1–2 μm, 2–3 μm, and 3–10 μm were produced by a nebulizer. The aerosol particles of NaCl and DEHS flowed through the composite at a flow rate of 2.0 m^3/h. The total measurement time was from 5 min to 12 h. The effective test area was 250 cm^2. There were two replicates for each group of tests. Filtration efficiency (E) was calculated based on Eq. (3) (Zhang et al. 2020),

$$E(\%) = \frac{(C_0 - C_t)}{C_0} \times 100 \quad (3)$$

where C_0 and C_t are the measured particle concentrations before and after filtration as recorded by an optical particle counter (LAP 322), respectively.

Quality factor (QF) is an indicator employed to evaluate the performances of the filters in terms of filtration efficiency and pressure drop. QF is defined as (Liu et al. 2021):

$$QF = -\ln(1 - \eta)/\Delta P \quad (4)$$

where η and ΔP are the filtration efficiency and pressure drop of the composite, respectively.

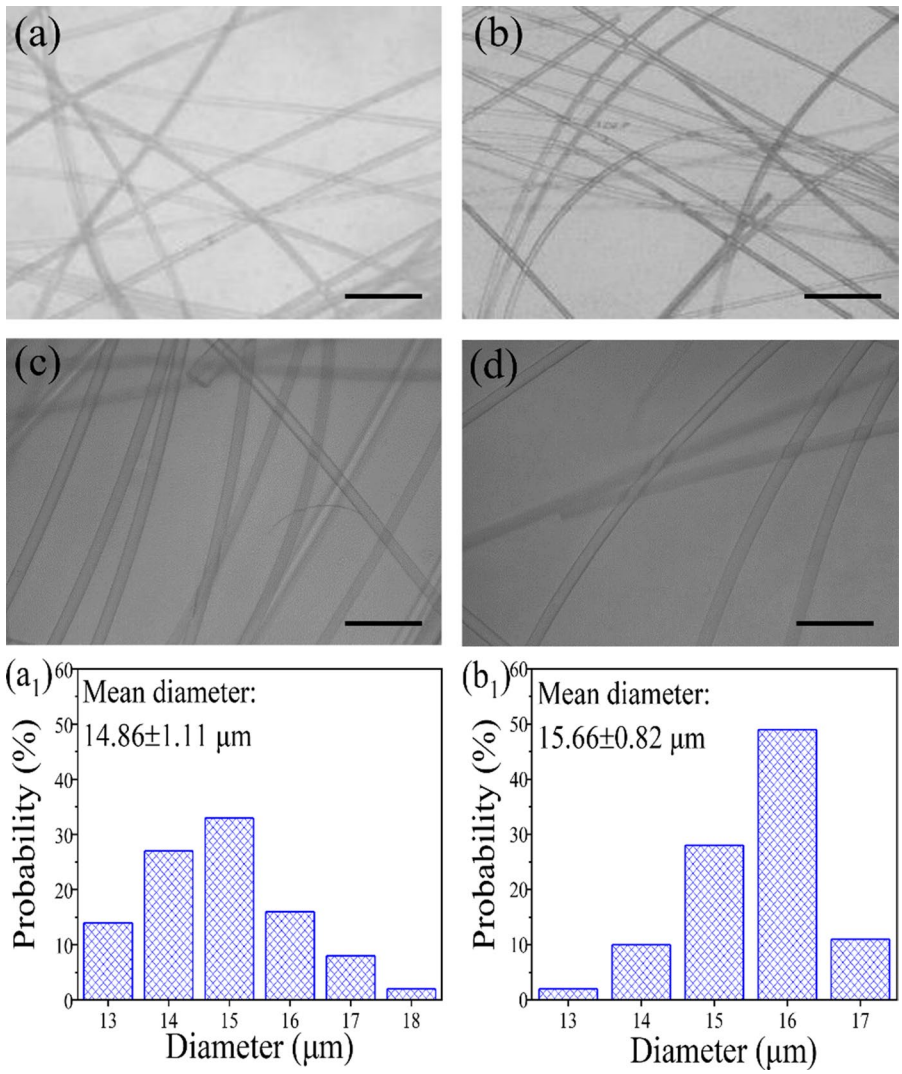

Fig. 2 Optical microscopy images of original lyocell fibres (**a**, **c**) S_0 and lyocell fibres pretreated with 2 wt% sodium hydroxide (**b**, **d**) S_2 (scale bars for a, b = 200 μm and c, d = 100 μm, respectively), along with diameter distribution of S_0 (a_1) and S_2 (b_1)

Results and discussion

Fibrillation of lyocell fibres

The original lyocell fibres had an average diameter of 14.86 μm, as shown in Fig. 2a, c and a1. Shear and friction forces acted on the fibres during the blending process (Wang et al. 2012; Wang et al. 2022a, b, c), leading to successful fibrillation of the lyocell fibres. During this process, 2 wt% NaOH was employed to pretreat the lyocell fibres for 24 h, and the swollen fibres were then successfully fibrillated under mechanical force. Fig. S2b shows peeling bundled microfibrils from the backbone of the lyocell fibres as well as splitting of the lyocell fibres into individual microfibrils. As demonstrated in Fig. 2, the results showed that the diameter of the pretreated lyocell fibres slightly increased to 15.66 μm (S_2) because of swelling. After mechanical treatment, the mean diameter of the fibrillated lyocell fibres pretreated by NaOH was smaller than that without NaOH pretreatment, as shown by comparisons of Fig. S3a_1 and S3d_1, Fig. S3b_1 and S3e_1, Fig. S3c_1 and S3f_1, Fig. S4a_1 and S4d_1, Fig. S4b_1 and S4e_1, and Fig. S4c_1 and S4f_1, which indicated that NaOH pretreatment has a positive effect on the fibrillation of the lyocell fibres.

As displayed in Fig. S4a_1-c_1, with increasing blending time from 3 to 9 min, the diameter distribution shifted to a smaller range, and the mean diameter decreased from 15.22 μm ($C_1R_2t_3$) to 13.62 μm ($C_1R_2t_6$) and 7.97 μm ($C_1R_2t_9$) in the absence of NaOH pretreatment. This demonstrated that blending time also had a significant effect on the diameter of the lyocell fibres. In contrast, when NaOH pretreatment was employed, with increasing blending time, the diameter variation of the lyocell fibres showed a similar trend but decreased to a lower level (Fig. S4d_1-f_1). The effect of blending rate on the diameter of lyocell fibres was explored. The diameter of the lyocell fibres pretreated with 2 wt% NaOH decreased from 15.66 μm (S_2) to 8.90 μm ($S_2C_1R_1t_9$), 7.49 μm ($S_2C_1R_2t_9$) and 6.02 μm ($S_2C_1R_3t_9$) with increasing blending rates of 12,000, 24,000 and 36,000 r/min for 9 min, or by 43.17%, 52.11% and 61.56%, respectively (Fig. S3d_1-f_1). A significant decrease in diameter was observed after mechanical treatment. A similar result was also observed for lyocell fibres not treated with NaOH, but the diameter was higher than that of the fibrillated fibres obtained from pretreated lyocell fibres, as demonstrated in Fig. S3a_1-c_1. It is worth noting that NaOH pretreatment not only reduced the diameter of fibrillated lyocell fibres but also decreased the polydispersity of the diameter distributions. For instance, the range of diameters decreased from 6.63 μm for $C_1R_3t_9$ to 6.02 μm for $S_2C_1R_3t_9$, as demonstrated in Fig. S3. Optical microscopy images and the diameter distributions of fibrillated lyocell fibres prepared by mechanical treatment for varied solid concentrations are shown in Fig. 3. Compared with samples prepared under the same conditions except with different solid conditions (Fig. 3a1 and d1, b1 and e1, c1 and f1), it was seen that a high solid concentration of 0.4 wt% facilitated a reduction in the diameter of fibrillated lyocell fibres. Specifically, the mean diameter of $S_2C_1R_2t_3$ pretreated by 2 wt% NaOH solution was 13.28 μm and decreased to 7.87 μm ($S_2C_4R_2t_3$) after the solid concentration was increased from 0.1 to 0.4 wt% with a mechanical treatment of 24,000 r/min for 3 min (Fig. 3a1 and d1). Similar results can be observed for $S_2C_1R_2t_6$ and $S_2C_4R_2t_6$ and for $S_2C_1R_2t_9$ and $S_2C_4R_2t_9$, as shown in Fig. 3. This is due to fibre–fibre friction, which is improved with increasing fibre consistency. The improved fibre–fibre friction and shear force induce pronounced diameter reduction.

Properties of the LC/PET composites

Based on the above results, the fibrillated lyocell fibres of $S_2C_4R_2t_3$, $S_2C_4R_2t_6$ and $S_2C_4R_2t_9$ were selected for further study since the three samples have relatively lower diameters, and the difference in their diameters was distinct. The composites were fabricated by filtering the mixed suspension of the lyocell fibres and polyester fibres using a pressurized filtration device. The overall filtration efficiency, pressure drop and QF of the as-prepared composites are displayed in Fig. 4. When the portion of fibrillated lyocell fibres mechanically treated for 3 min was 100%, the overall filtration efficiency of the composite with a basis weight of 40 g/m^2 was 99.87% ($P_{100}W_{40}t_3$). However, the pressure drop reached 741.00 Pa, which indicated the poor permeability of the composite. This is because the fibrillation of the lyocell fibres resulted in greater exposure of hydroxyl groups, which forms hydrogen bonds. Hence, the structure of the composite was very compact, leading to poor permeability. To decrease the pressure drop, PET fibres were mixed

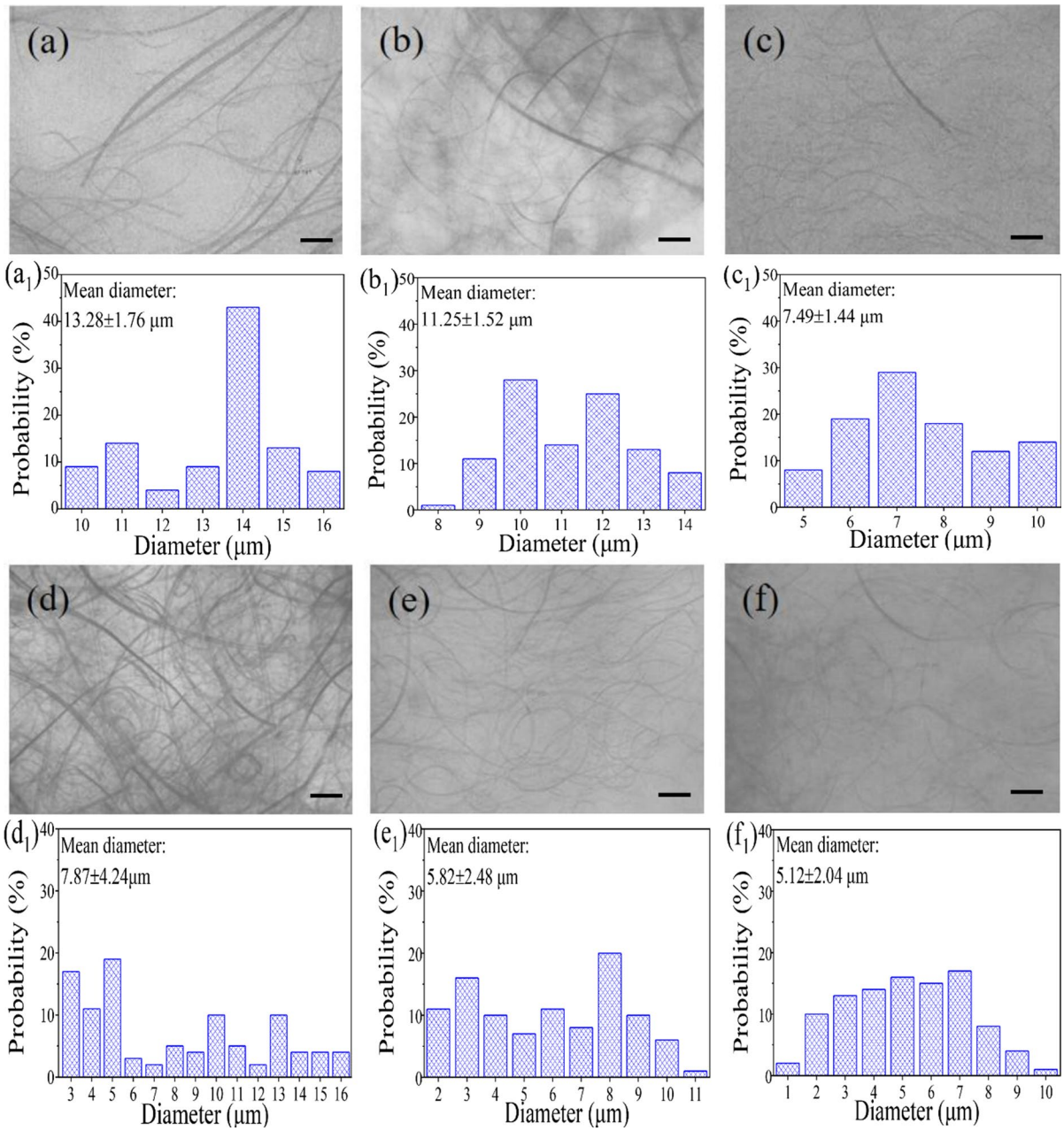

Fig. 3 Optical microscopy image of the lyocell fibres after blending with different fibre concentrations: **a** $S_2C_1R_2t_3$; **b** $S_2C_1R_2t_6$; **c** $S_2C_1R_2t_9$; **d** $S_2C_4R_2t_3$; **e** $S_2C_4R_2t_6$; **f** $S_2C_4R_2t_9$. The scale of the optical microscopy image corresponds to 100 μm, and the corresponding diameter distributions are (a_1-f_1)

as spacers between the fibrillated lyocell fibres. With a decrease in the lyocell fibre proportion from 100 to 20%, the pressure drop significantly decreased to 17.50 Pa ($P_{20}W_{40}t_3$). However, the filtration efficiency was markedly decreased to 21.55% (Fig. 4a, c). This is because the addition of PET fibres increased the distance between hydrogen and oxygen atoms on the hydroxyl groups of lyocell fibres, hindering the formation of intermolecular hydrogen bonds. In addition, PET does not have functional groups that can

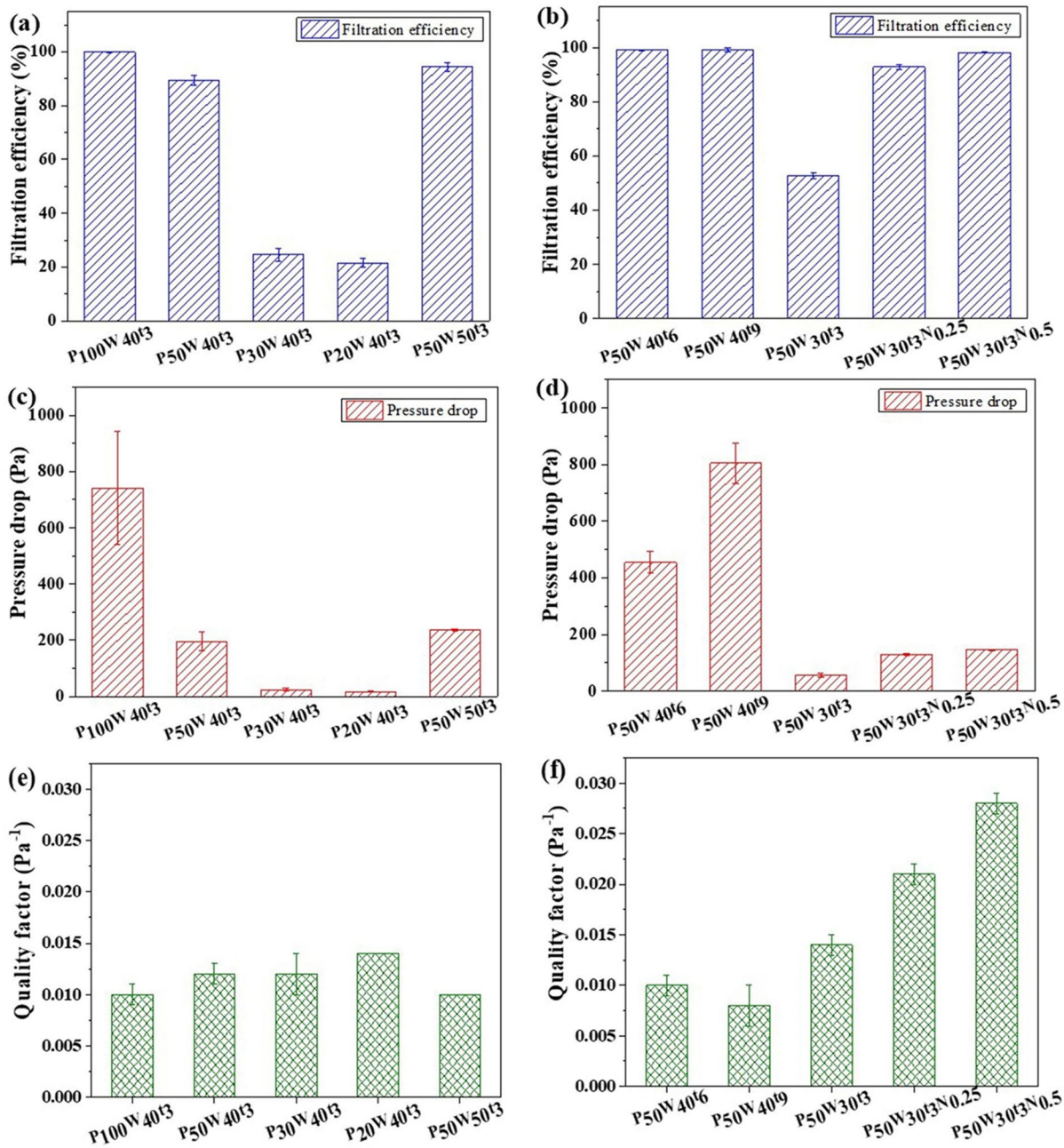

Fig. 4 Properties of different air filter composites. **a**–**d** Overall filtration efficiency and pressure drop and **e**, **f** QF

form hydrogen bonds with hydroxyl groups on the surface of the lyocell fibres. Hence, the structure of the composite became less compact. Inspection of the thickness, density and pore diameter of the composites confirmed the above results, as displayed in Fig. 5 and Table 1. The thickness of the composites gradually increased from 144.98 ($P_{100}W_{40}t_3$) to 240.64 μm ($P_{20}W_{40}t_3$), while the density decreased from 0.26 ($P_{100}W_{40}t_3$) to 0.15 g/cm^3 ($P_{20}W_{40}t_3$). The variation in the thickness and density of the composites validated that their structure became looser with an increase in the proportion of PET fibres from 0 to

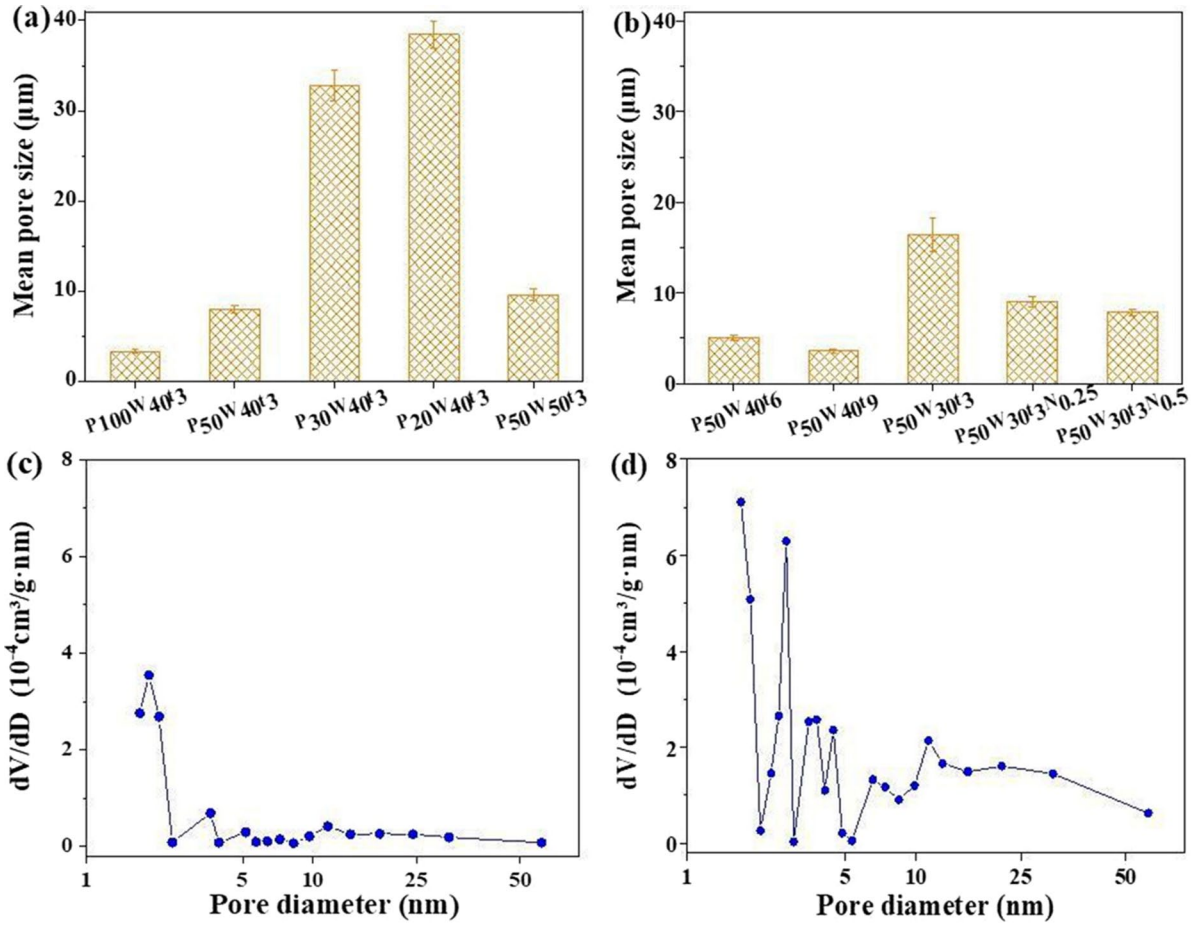

Fig. 5 **a**, **b** Mean pore size of different composites, the pore size distribution of **c** $P_{50}W_{30}t_3$ and **d** $P_{50}W_{30}t_3N_{0.5}$

Table 1 The thickness and density of the composites

Composites	Thickness (mm)	Density (g/cm^3)
$P_{100}W_{40}t_3$	144.98 ± 18.24	0.26 ± 0.04
$P_{50}W_{40}t_3$	182.18 ± 25.89	0.22 ± 0.04
$P_{30}W_{40}t_3$	190.53 ± 17.67	0.20 ± 0.02
$P_{20}W_{40}t_3$	240.64 ± 12.83	0.15 ± 0.02
$P_{50}W_{40}t_6$	146.04 ± 13.14	0.27 ± 0.03
$P_{50}W_{40}t_9$	155.35 ± 10.64	0.26 ± 0.02
$P_{50}W_{30}t_3$	131.67 ± 15.98	0.23 ± 0.04
$P_{50}W_{30}t_3N_{0.25}$	200.34 ± 24.29	0.15 ± 0.02
$P_{50}W_{30}t_3N_{0.5}$	180.87 ± 24.14	0.17 ± 0.03
$P_{50}W_{50}t_3$	316.65 ± 56.41	0.16 ± 0.03

80%. Furthermore, the mean pore size of the composites increased markedly from 3.30 ($P_{100}W_{40}t_3$) to 38.46 μm ($P_{20}W_{40}t_3$) (Fig. 5), indicating that the PET fibres increased the spacing between the fibrillated lyocell fibres.

The effect of the diameter of the fibrillated lyocell fibres on the performance of the composite was studied. The diameters of the obtained lyocell fibres were 7.87 μm ($S_2C_4R_2t_3$), 5.82 μm ($S_2C_4R_2t_6$) and 5.12 μm ($S_2C_4R_2t_9$) (Fig. 3). As the blending time increased from 3 to 6 min, the overall filtration efficiency of the composites with a basis weight of 40 g/m^2 (LC/PET = 50 wt%:50 wt%) increased from 89.47% ($P_{50}W_{40}t_3$) to 98.96% ($P_{50}W_{40}t_6$), but the pressure drop significantly increased from 195.67 to 454.50 Pa. Further extending the blending time to 9 min slightly increased the overall filtration

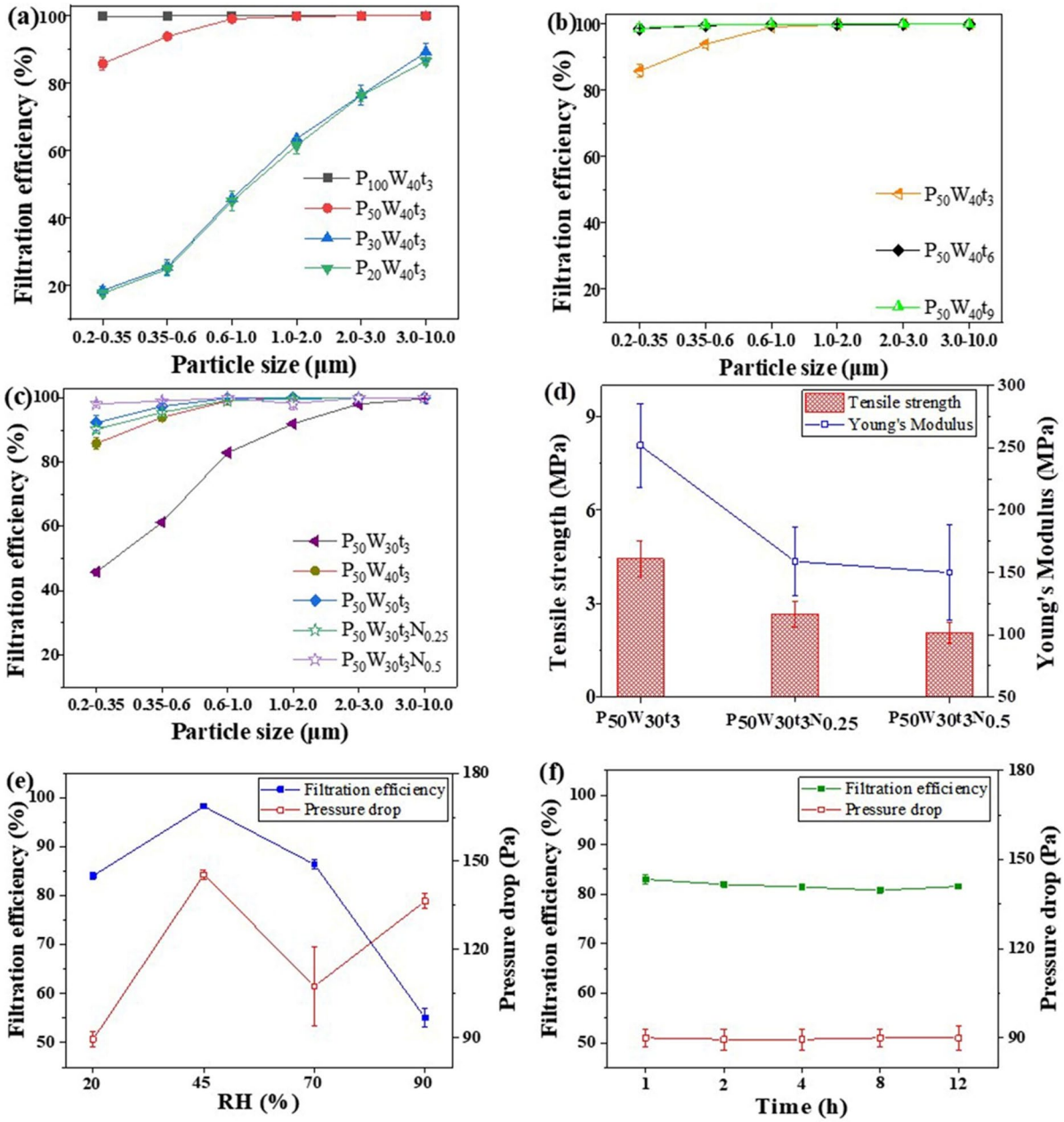

Fig. 6 **a–c** Filtration efficiency of different air filter composites for various particle sizes of PM, **d** mechanical properties of different air filter composites, filtration efficiency and pressure drop of composite of $P_{50}W_{30}t_3N_{0.5}$ under different RHs **e** and **f** times.

efficiency to 99.13%. However, the pressure drop noticeably increased to 805.00 Pa. The diameter of the lyocell fibres decreased, and the extent of fibrillation increased with increasing blending time, resulting in greater exposure of hydroxyl groups. Therefore, more hydrogen bonding led to a more compact structure in the LC/PET composites, which was verified by measurements of the variations in thickness, density and mean pore size. The thickness of the composites decreased from 182.18 ($P_{50}W_{40}t_3$) to 155.35 μm ($P_{50}W_{40}t_9$) with increasing treatment time from 3 to 9 min. In turn, the density improved from

0.22 to 0.26 g/cm^3 (Table 1). The mean pore size of the composites decreased from 7.96 ($P_{50}W_{40}t_3$) to 3.59 µm ($P_{50}W_{40}t_9$) (Fig. 5, 6), indicating more coalescence of the fibre network. This is the reason why the filtration efficiency and pressure drop improved with extended blending time. Upon increasing the basis weight of the composites from 30 to 50 g/m^2, the overall filtration efficiency increased significantly from 52.69% ($P_{50}W_{30}t_3$) to 94.42% ($P_{50}W_{50}t_3$) with a considerable increase in the pressure drop from 56.50 Pa to 237.00 Pa owing to the increased thickness of the composites (Fig. 4).

Improvement in the quality factor of composites by impregnating CNFs in LC/PET composites

QF represents the comprehensive performance of air filter composites. As shown in Fig. 4, the composites of $P_{50}W_{40}t_3$ and $P_{50}W_{50}t_3$ possessed a relatively high filtration efficiency and acceptable pressure drop. However, the QFs of $P_{50}W_{40}t_3$ and $P_{50}W_{50}t_3$ were only 0.012 and 0.010 Pa^{-1}, respectively. Hence, CNFs were incorporated in the LC/PET composites to construct hierarchical structures to improve filtration efficiency as well as the QF. Figure 1 demonstrates the process of incorporating CNFs into LC/PET composites. As displayed in Fig. 4, the composite of $P_{50}W_{30}t_3$ exhibited moderate filtration efficiency and a low pressure drop. Hence, it was selected as the substrate to build porous LC/PET/CNF composites. The results showed that both composites $P_{50}W_{30}t_3N_{0.25}$ and $P_{50}W_{30}t_3N_{0.5}$ achieved remarkable filtration efficiencies of 92.80% and 98.22%, respectively, along with excellent QFs of 0.021 and 0.028 Pa^{-1} after incorporation of CNFs. This occurred possibly because the LC/PET/CNF composites possess a more porous network and smaller pores than the LC/PET composites. During freezing in liquid nitrogen after was suspension of CNFs was sprayed on the composite of $P_{50}W_{30}t_3$, small ice crystals formed due to the rapid freezing, yielding a porous structure with small pores in the LC/PET/CNF composites after the ice crystals sublimated (Qin et al. 2021). The mean pore sizes of $P_{50}W_{30}t_3N_{0.25}$ and $P_{50}W_{30}t_3N_{0.5}$ were 9.04 and 7.87 µm, respectively, which were smaller than that of $P_{50}W_{30}t_3$ (16.39 µm), validating the successful construction of the hierarchical structure of the LC/PET/CNF composites. Most of the fibres observed were on the micrometre scale before incorporation of CNFs (Fig. 7a and a1). However, after implantation of the CNFs, a fluffy network including both nano- and micrometre-scale fibres was observed (Fig. 7b and b1, c and c_1). The pore size in $P_{50}W_{30}t_3$ was larger than that in $P_{50}W_{30}t_3N_{0.25}$ and $P_{50}W_{30}t_3N_{0.5}$. The smaller networks in the LC/PET composite of $P_{50}W_{30}t_3$ facilitated the interception and adsorption of PM, leading to a remarkable improvement in filtration efficiency (Qin et al. 2021). In addition, the pressure drops of $P_{50}W_{30}t_3N_{0.25}$ and $P_{50}W_{30}t_3N_{0.5}$ were 129.50 and 145.50 Pa, respectively, which were significantly lower than those of the composites with similar filtration efficiencies. For instance, the overall filtration efficiency of $P_{50}W_{40}t_6$ was 98.96%, with a high pressure drop of 454.50 Pa. The pressure drop of the LC/PET/CNF composites was lower because of low density relative to that of the LC/PET composites (Table 1). Because of the high filtration efficiency and low pressure drop, the LC/PET/CNF composites achieved a high QF of 0.021 Pa^{-1} for $P_{50}W_{30}t_3N_{0.25}$ and 0.028 Pa^{-1} for $P_{50}W_{30}t_3N_{0.5}$. The filtration efficiency of the composite of $P_{50}W_{30}t_3N_{0.5}$ was determined under different RHs (Fig. 6e). When the RH reached 90%, the filtration efficiency of the air filter declined dramatically. This may be because of the collapse of the network structure of CNFs (Xiong et al. 2021). The filtration efficiency of the composite was explored at 20% RH as a function of filtration time, as displayed in Fig. 6f. The results showed that the filtration efficiency remained almost unchanged for all measurement times, indicating effective filtration of PM. The tensile strength and Young's modulus were measured as displayed in Fig. 6d. As the concentration of CNFs increased from 0 to 0.25 and 0.5 g/m^2, the tensile strength of the air filter decreased from 4.43 MPa ($P_{50}W_{30}t_3$) to 2.67 MPa ($P_{50}W_{30}t_3N_{0.25}$) and 2.05 MPa ($P_{50}W_{30}t_3N_{0.5}$), while the Young's modulus significantly decreased from 251.80 MPa ($P_{50}W_{30}t_3$) to 158.80 MPa ($P_{50}W_{30}t_3N_{0.25}$) and 149.89 MPa ($P_{50}W_{30}t_3N_{0.5}$) (Fig. 6d), respectively. This is because the structure of the air filter became looser and more porous after implantation of CNFs, impacting the bonding of the fibres.

As shown in Fig. 6a–c, it is obvious that the filtration efficiency of composites was higher for larger particles than for smaller particles. For particles with a size range of 1–10 µm, inertial impaction dominated particle removal. Owing to their large mass, large particles fail to follow the

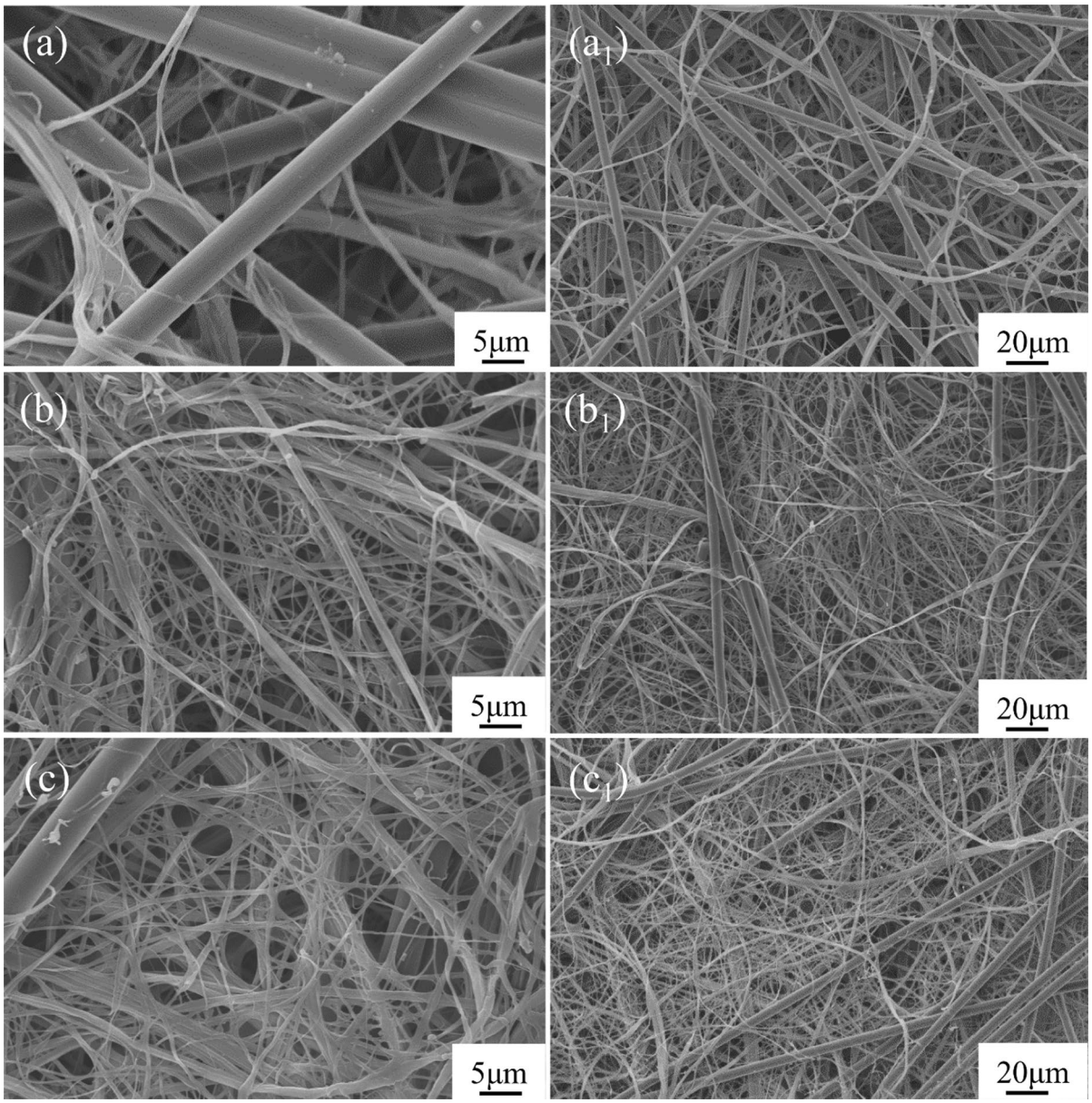

Fig. 7 SEM images of (**a**, **a**$_1$) $P_{50}W_{30}t_3$, (**b**, **b**$_1$) $P_{50}W_{30}t_3N_{0.25}$ and (**c**, **c**$_1$) $P_{50}W_{30}t_3N_{0.5}$

curved paths of the air streamlines around fibres, and they collide with the fibres. Hence, the particles were captured by the fibres by inertial impaction, which explains why the filtration efficiency for larger particles with high inertial force is typically higher. For particles with a size of 0.1–1 μm, mechanical interception of the particles by filter fibres plays a major role. Interception occurs when a particle flows with the airflow and then hits a fibre. Therefore, the particle binds to fibres and is removed from the airflow. Diffusion caused by Brownian motion is the dominant mechanism for particles at the nanoscale, especially for particles smaller than 0.1 μm. A particle deviates from its original streamline randomly owing to Brownian motion, and the particle can be caught immediately once the departure is sufficient, which allows collision between the particle and a fibre (Zhu et al. 2017; Tan et al. 2019; Konda

et al. 2020). The filtration efficiency of $P_{50}W_{30}t_3$ for particles with a size of 0.2–1 μm was in the range of 51.75–53.63%, while the filtration efficiency was noticeably improved to the range of 98.06–98.38% after a suspension of CNFs was sprayed on $P_{50}W_{30}t_3$. This is because the presence of the CNFs resulted in a more porous network with smaller pore sizes, which increased the probability of particle deposition, enhancing the mechanical interception of particles with a size of 0.2–1 μm by fibres. The specific surface area and pore volume of the composites of $P_{50}W3_0t_3$, $P_{50}W_3t_{30}N_{0.25}$ and $P_{50}W_{30}t_3N_{0.5}$ were measured (Table S3). As the concentration of CNFs increased from 0 to 0.5 g/m^2, the specific surface area of the air filter composites increased from 1.53 m^2/g ($P_{50}W_{30}t_3$) to 5.24 m^2/g ($P_{50}W_{30}t_3N_{0.5}$), while the pore volumes improved from 0.0034 to 0.0164 cm^3/g. This means that the addition of CNFs increases the porosity of the filter, improving its filtration performance.

Conclusion

In summary, hierarchically structured LC/PET/CNF composites were constructed using pressurized filtration followed by spraying. The size of the fibrillated lyocell fibres used for the fabrication of composites could be controlled by changing blending conditions, including the blending rate, time and solid concentration of the fibre suspension. The filtration efficiency and pressure drop of the LC/PET composites were regulated by altering the size of the fibrillated lyocell fibres, basis weight of the composites and LC/PET ratio. However, although the overall filtration efficiency of the LC/PET composite ($P_{50}W_{40}t_3$) reached 89.47%, the pressure drop reached 195.67 Pa, with a low QF of 0.012 Pa^{-1}. After a suspension of CNFs was sprayed on the LC/PET composite ($P_{50}W_{30}t_3$), the subsequently freeze-dried LC/PET/CNF composites displayed a hierarchical porous structure with smaller pore sizes, which greatly increased the possibility of interception of small particles with sizes 0.1–1 μm and the inertial impaction of particles larger than 1–10 μm. Thus, the overall filtration efficiency of $P_{50}W_{30}t_3N_{0.5}$ was improved to 98.22% from 52.69% ($P_{50}W_{30}t_3$). With the support of the CNFs in the LC/PET composites, $P_{50}W_{30}t_3N_{0.5}$ exhibited a lower density and higher thickness than $P_{50}W_{30}t_3$, resulting in a lower pressure drop of 145.50 Pa and a high QF of 0.028 Pa^{-1}, with superhigh filtration efficiency. The study provides new insights into the preparation of high-performance air filter composites.

Acknowledgments The work was supported by the Key Research and Development Program of Shandong Province (2020CXGC011101), the Natural Science Foundation of Shandong Province (ZR2019QEM007 and ZR2020ME076), the State Key Laboratory of Bio-Fibres and Eco-Textiles (Qingdao University) (KF2020209, ZKT08, ZKT16, ZKT18 and ZKT21), the Undergraduate Innovation and Entrepreneurship Training Program of Qingdao University (S202011065011), and the Special Foundation of "Taishan Scholar" Construction Program.

Author contributions All authors contributed to the study conception and design. Material preparation, data collection and analysis were performed by J.W. Zhang. The first draft of the manuscript was written by J.W. Zhang, and X.J. Wang commented on subsequent versions of the manuscript. All authors read and approved the final manuscript.

Funding The Key Research and Development Program of Shandong Province (2020CXGC011101), the Natural Science Foundation of Shandong Province (ZR2019QEM007 and ZR2020ME076), the State Key Laboratory of Bio-Fibres and Eco-Textiles (Qingdao University) (KF2020209, ZKT08, ZKT16, ZKT18 and ZKT21), the Undergraduate Innovation and Entrepreneurship Training Program of Qingdao University (S202011065011), and the Special Foundation of "Taishan Scholar" Construction Program.

Data availability All relevant data are within the manuscript, which is available from the corresponding author upon request.

Declarations

Competing interests The authors have no relevant financial or nonfinancial interests to disclose.

Ethics approval and consent to participate This article does not contain any studies or investigations conducted by the authors on human participants or animals that violate ethical standards.

Consent for publication The authors agree to publish the article under the Creative Commons Attribution Licence.

References

Avossa J, Batt T, Pelet T, Sidjanski SP, Schönenberger K, Rossi RM (2021) Polyamide nanofiber-based air filters for

transparent face masks. ACS Appl Nano Mater 4:12401–12406. https://doi.org/10.1021/acsanm.1c02843

Balgis R, Murata H, Goi Y, Ogi T, Okuyama K, Bao L (2017) Synthesis of dual-size cellulose-polyvinylpyrrolidone nanofiber composites via one-step electrospinning method for high-performance air filter. Langmuir 33:6127–6134. https://doi.org/10.1021/acs.langmuir.7b01193

Beaumont M, Bacher M, Opietnik M, Gindl-Altmutter W, Potthast A, Rosenau T (2018) A general aqueous silanization protocol to introduce vinyl, mercapto or azido functionalities onto cellulose fibers and nanocelluloses. Molecules 23:1427. https://doi.org/10.3390/molecules23061427

Farooq M, Zou T, Riviere G, Sipponen MH, Österberg M (2019) Strong, ductile, and waterproof cellulose nanofibril composite films with colloidal lignin particles. Biomacromol 20:693–704. https://doi.org/10.1021/acs.biomac.8b01364

Gu GQ, Han CB, Lu CX, He C, Jiang T, Gao ZL, Li CJ, Wang ZL (2017) Triboelectric nanogenerator enhanced nanofiber air filters for efficient particulate matter removal. ACS Nano 11:6211–6217. https://doi.org/10.1021/acsnano.7b02321

Han SO, Son WK, Youk JH, Park WH (2008) Electrospinning of ultrafine cellulose fibers and fabrication of poly(butylene succinate) biocomposites reinforced by them. J Appl Polym Sci 107:1954–1959. https://doi.org/10.1002/app.26643

Heggset EB, Chinga-Carrasco G, Syverud K (2017) Temperature stability of nanocellulose dispersions. Carbohydr Polym 157:114–121. https://doi.org/10.1016/j.carbpol.2016.09.077

Hoeng F, Denneulin A, Krosnicki G, Bras J (2016) Positive impact of cellulose nanofibrils on silver nanowire coatings for transparent conductive films. J Mater Chem C Mater 4:1945–1954. https://doi.org/10.1039/c6tc03629e

Kiss P, Stadlbauer W, Burgstaller C, Archodoulaki V (2020) Development of high-performance glass fibre-polypropylene composite laminates: effect of fibre sizing type and coupling agent concentration on mechanical properties. Composites Part A 138:106056. https://doi.org/10.1016/j.compositesa.2020.106056

Konda A, Prakash A, Moss G, Schmoldt M, Grant G, Guha S (2020) Correction to aerosol filtration efficiency of common fabrics used in respiratory cloth masks. ACS Nano 14:10742–10743. https://doi.org/10.1021/acsnano.0c04676

Lavoine N, Bergström L (2017) Nanocellulose-based foams and aerogels: processing, properties, and applications. J Mater Chem A Mater 5:1615–16117. https://doi.org/10.1039/c7ta02807e

Li Q, Wu Y, Fang R, Lei C, Li Y, Li B, Pei Y, Luo X, Liu S (2021) Application of nanocellulose as particle stabilizer in food pickering emulsion: scope, merits and challenges. Trends Food Sci Technol 110:573–583. https://doi.org/10.1016/j.tifs.2021.02.027

Liu T, Cai C, Ma R, Deng Y, Tu L, Fan Y, Lu D (2021) Superhydrophobic cellulose nanofiber air filter with highly efficient filtration and humidity resistance. ACS Appl Mater Interfaces 13:24032–24041. https://doi.org/10.1021/acsami.1c04258

Long J, Tang M, Liang Y, Hu J (2018) Preparation of fibrillated cellulose nanofiber from lyocell fiber and its application in air filtration. Materials (Basel) 11:1313. https://doi.org/10.3390/ma11081313

Ma S, Zhang M, Nie J, Yang B, Song S, Lu P (2018) Multifunctional cellulose-based air filters with high loadings of metal-organic frameworks prepared by in situ growth method for gas adsorption and antibacterial applications. Cellulose (Lond) 25:5999–6010. https://doi.org/10.1007/s10570-018-1982-1

Maiti S, Jayaramudu J, Das K, Reddy SM, Sadiku R, Ray SS, Liu D (2013) Preparation and characterization of nanocellulose with new shape from different precursor. Carbohydr Polym 98:562–567. https://doi.org/10.1016/j.carbpol.2013.06.029

Nata IF, Wu T, Chen J, Lee C (2014) A chitin nanofibril reinforced multifunctional monolith poly(vinyl alcohol) cryogel. J Mater Chem B 2:4108–4113. https://doi.org/10.1039/C4TB00175C

Navarro JRG, Wennmalm S, Godfrey J, Breitholtz M, Edlund U (2016) Luminescent nanocellulose platform: from controlled graft block copolymerization to biomarker sensing. Biomacromol 17:1101–1109. https://doi.org/10.1021/acs.biomac.5b01716

Navarro JRG, Rostami J, Ahlinder A, Mietner JB, Bernin D, Saake B, Edlund U (2020) Surface-initiated controlled radical polymerization approach to in situ cross-link cellulose nanofibrils with inorganic nanoparticles. Biomacromol 21:1952–1961. https://doi.org/10.1021/acs.biomac.0c00210

Pant HR, Pant B, Pokharel P, Kim HJ, Tijing LD, Park CH, Lee DS, Kim HY, Kim CS (2013) Photocatalytic TiO_2-RGO/nylon-6 spider-wave-like nano-nets via electrospinning and hydrothermal treatment. J Membr Sci 429:225–234. https://doi.org/10.1016/j.memsci.2012.11.025

Park M, Kuk Y, Kwon OH, Acharya J, Ojha GP, Ko J, Kong H, Pant B (2022) Fly ash-incorporated polystyrene nanofiber membrane as a fire-retardant material: valorization of discarded materials. Nanomaterials (Basel) 12:3811. https://doi.org/10.3390/nano12213811

Qin H, Zhang Y, Jiang J, Wang L, Song M, Bi R, Zhu P, Jiang F (2021) Multifunctional superelastic cellulose nanofibrils aerogel by dual ice-templating assembly. Adv Funct Mater 31:2106269. https://doi.org/10.1002/adfm.202106269

Ren Y, Luo Q, Zhuo S, Hu Y, Shen G, Cheng H, Tao S (2021) Bioaccessibility and public health risk of heavy Metal(loid)s in the airborne particulate matter of four cities in northern China. Chemosphere 277:130312. https://doi.org/10.1016/j.chemosphere.2021.130312

Shi S, Zhi C, Zhang S, Yang J, Si Y, Jiang Y, Ming Y, Lau K, Fei B, Hu J (2022) Lotus leaf-inspired breathable membrane with structured microbeads and nanofibers. ACS Appl Mater Interfaces 14:39610–39621. https://doi.org/10.1021/acsami.2c11251

Souzandeh H, Scudiero L, Wang Y, Zhong W (2017) A disposable multi-functional air filter: paper towel/protein nanofibers with gradient porous structures for capturing pollutants of broad species and sizes. ACS Sustainable Chem Eng 5:6209–6217. https://doi.org/10.1021/acssuschemeng.7b01160

Tan NPB, Paclijan SS, Ali HNM, Hallazgo CMJS, Lopez CJF, Ebora YC (2019) Solution blow spinning (SBS) nanofibers for composite air filter masks. ACS Appl Nano Mater 2:2475–2483. https://doi.org/10.1021/acsanm.9b00207

Thakur VK, Thakur MK (2014) Processing and characterization of natural cellulose fibers/thermoset polymer composites. Carbohydr Polym 109:102–117. https://doi.org/10.1016/j.carbpol.2014.03.039

Tu H, Zhu M, Duan B, Zhang L (2021) Recent progress in high-strength and robust regenerated cellulose materials. Adv Mater 33:2000682. https://doi.org/10.1002/adma.202000682

Wang QQ, Zhu JY, Gleisner R, Kuster TA, Baxa U, McNeil SE (2012) Morphological development of cellulose fibrils of a bleached eucalyptus pulp by mechanical fibrillation. Cellulose (Lond) 19:1631–1643. https://doi.org/10.1007/s10570-012-9745-x

Wang L, Chen C, Wang J, Gardner DJ, Tajvidi M (2020) Cellulose nanofibrils versus cellulose nanocrystals: comparison of performance in flexible multilayer films for packaging applications. Food Packag Shelf Life 23:100464. https://doi.org/10.1016/j.fpsl.2020.100464

Wang X, Li R, Zeng J, Cheng Z, Wang B, Ding Q, Gao W, Chen K, Xu J (2020b) Efficient fractionation of cellulose nanofibers using spiral microchannel. Cellulose (Lond) 27:4029–4041. https://doi.org/10.1007/s10570-020-03072-2

Wang X, Xiang H, Song C, Zhu D, Sui J, Liu Q, Long Y (2020) Highly efficient transparent air filter prepared by collecting-electrode-free bipolar electrospinning apparatus. J Hazard Mater 385:121535. https://doi.org/10.1016/j.jhazmat.2019.121535

Wang D, Zhang D, Li P, Yang Z, Mi Q, Yu L (2021) Electrospinning of flexible poly(vinyl alcohol)/MXene nanofiber-based humidity sensor self-powered by monolayer molybdenum diselenide piezoelectric nanogenerator. Nanomicro Lett 13:57. https://doi.org/10.1007/s40820-020-00580-5

Wang Q, Liu S, Liu J, Sun J, Zhang Z, Zhu Q (2022) Sustainable cellulose nanomaterials for environmental remediation-achieving clean air, water, and energy: a review. Carbohydr Polym 285:119251. https://doi.org/10.1016/j.carbpol.2022.119251

Wang Q, Liu S, Liu J, Sun J, Zhang Z, Zhu Q (2022) Sustainable cellulose nanomaterials for environmental remediation-achieving clean air, water, and energy: a review. Carbohydr Polym 285:119251. https://doi.org/10.1016/j.carbpol.2022.119251

Wang X, Zeng J, Zhu JY (2022) Morphological and rheological properties of cellulose nanofibrils prepared by post-fibrillation endoglucanase treatment. Carbohydr Polym 295:119885. https://doi.org/10.1016/j.carbpol.2022.119885

Watanabe K, Maeda T, Hotta A (2018) Uniformly dispersed polymeric nanofiber composites by electrospinning: poly(vinyl alcohol) nanofibers/polydimethylsiloxane composites. Compos Sci Technol 165:18–23. https://doi.org/10.1016/j.compscitech.2018.06.007

White AJ, Kresovich JK, Keller JP, Xu Z, Kaufman JD, Weinberg CR, Taylor JA, Sandler DP (2019) Air pollution, particulate matter composition and methylation-based biologic age. Environ Int 132:105071. https://doi.org/10.1016/j.envint.2019.105071

Wu X, Chen S, Guo J, Gao G (2018) Effect of air pollution on the stock yield of heavy pollution enterprises in China's key control cities. J Clean Prod 170:399–406. https://doi.org/10.1016/j.jclepro.2017.09.154

Xiong Z, Lin J, Li X, Bian F, Wang J (2021) Hierarchically structured nanocellulose-implanted air filters for high-efficiency particulate matter removal. ACS Appl Mater Interfaces 13:12408–12416. https://doi.org/10.1021/acsami.1c01286

Xiong Z, Li X, Wang J, Lin J (2022) Nanocellulose implantation enriched the pore structure of aerogel for effective particulate matter removal. Int J Biol Macromol 219:1237–1243. https://doi.org/10.1016/j.ijbiomac.2022.08.188

Xu H, Jin W, Luo J, Wang F, Zhu H, Liu G, Yu Y, Lei C, Guo Y (2021) Study of the PTFE multi-tube high efficiency air filter for indoor air purification. Process Saf Environ Prot 151:28–38. https://doi.org/10.1016/j.psep.2021.05.007

Zhang R, Liu C, Hsu P, Zhang C, Liu N, Zhang J, Lee HR, Lu Y, Qiu Y, Chu S, Cui Y (2016) Nanofiber air filters with high-temperature stability for efficient $PM_{2.5}$ removal from the pollution sources. Nano Lett 16:3642–3649. https://doi.org/10.1021/acs.nanolett.6b00771

Zhang X, Zhao X, Xue T, Yang F, Fan W, Liu T (2020) Bidirectional anisotropic polyimide/bacterial cellulose aerogels by freeze-drying for super-thermal insulation. Chem Eng J 385:123963. https://doi.org/10.1016/j.cej.2019.123963

Zhu M, Han J, Wang F, Shao W, Xiong R, Zhang Q, Pan H, Yang Y, Samal SK, Zhang F, Huang C (2017) Electrospun nanofibers membranes for effective air filtration. Macromol Mater Eng 302:1600353. https://doi.org/10.1002/mame.201600353